



HAL
open science

Tracer dispersion in a duct: Experimental and numerical approach – Application to the well-mixing length determination

Thomas Gelain, Jonathan Alengry, Olivier Vauquelin, Laurent Ricciardi

► To cite this version:

Thomas Gelain, Jonathan Alengry, Olivier Vauquelin, Laurent Ricciardi. Tracer dispersion in a duct: Experimental and numerical approach – Application to the well-mixing length determination. Nuclear Engineering and Design, 2019, 353, pp.110229. 10.1016/j.nucengdes.2019.110229 . hal-02457226

HAL Id: hal-02457226

<https://hal.science/hal-02457226v1>

Submitted on 27 Jan 2020

HAL is a multi-disciplinary open access archive for the deposit and dissemination of scientific research documents, whether they are published or not. The documents may come from teaching and research institutions in France or abroad, or from public or private research centers.

L'archive ouverte pluridisciplinaire **HAL**, est destinée au dépôt et à la diffusion de documents scientifiques de niveau recherche, publiés ou non, émanant des établissements d'enseignement et de recherche français ou étrangers, des laboratoires publics ou privés.



Distributed under a Creative Commons Attribution - NonCommercial - NoDerivatives 4.0 International License

Tracer dispersion in a duct: experimental and numerical approach - Application to the well-mixing length determination

Thomas Gelain ¹, Jonathan Alengry ¹, Olivier Vauquelin ², Laurent Ricciardi ¹

¹ *Institut de Radioprotection et de Sûreté Nucléaire (IRSN), PSN-RES, SCA, LEMAC, Saclay, Gif-sur-Yvette, 91192, France*

² *Aix-Marseille Université, Laboratoire IUSTI, UMR CNRS 7343, 5 rue Enrico Fermi, 13453 Marseille Cedex 13, France*

Abstract:

The aim of this study is to propose an analytical model for assessing the well-mixing length of a tracer in a ventilation duct.

The first part of the article is devoted to describe an experimental bench developed for validating the proposed model. This bench allows to follow the evolution of a tracer injected at a source point in the center of a duct by using an original optical measurement technique.

In a second part, an analytical model for the spatial evolution of a tracer concentration in a circular duct is developed, taking into account an eddy viscosity model.

The difficulty for applying this model to industrial cases led us to propose a simplified version that can be used for a non-dimensional distance greater than 20 diameters. The latter was then inverted in order to access to two criteria: the coefficient of variation in the duct section and the difference between the local measured concentration and the expected homogeneous concentration. Each one has its interest depending on whether a global information on the duct section or a local information (on the axis for example) at a given distance is required.

Keywords: well-mixing length, analytical model, tracer, duct

1 INTRODUCTION

In the nuclear industry, the monitoring of gaseous releases into the environment is based on contaminant concentration measurements in the discharge chimney, that require an appropriate implementation of the sampling point. Indeed, due to the mixing of effluents arising from the different extraction networks of a nuclear facility, the contaminant concentration may be heterogeneous in the top of the chimney if the length allowed for establishing the gaseous mixing is insufficient; the measurement performed may thus not be representative of the average concentration. Furthermore, periodic controls of the HEPA (High Efficiency Particulate Air) filters of the last filtration level, representing the final step of the gaseous effluent treatment system before discharge, use a normalized method that implements a test aerosol corresponding to the most penetrating particle size (PMMS), for example the soda fluorescein aerosol in FRANCE. This method requires a certain distance, known as the “well-mixing length”, between the injection and sampling points of the tracer upstream and downstream of the filter. Based on these samples, the decontamination factor of the filter can be calculated.

The well-mixing length is defined when the tracer concentration is homogeneous in the whole section of the pipe. In theory, this length is infinite, but practically, the positions of the sampling points are constrained by the configuration of the ventilation networks.

The problem of interest is either to be able to evaluate the well-mixing length in order to use it as well as possible in situ or, due to in situ constraints, to evaluate the tracer mixing heterogeneity and the induced error in case of local measurement. Ultimately, models should be developed for assessing in a restricted time the well-mixing length and the concentration heterogeneity in a section.

To this end, experimental data of tracer concentrations are needed and a dedicated experimental bench was developed. In preparation, bibliographic research was conducted to inventory similar studies on turbulent mixing in ducts. In the second half of the 20th century, this topic was much studied and Taylor (1954) was one of the first researchers to study the issue of turbulent mixing in pipes. His work consisted in following the evolution of a tracer pulse in smooth and rough pipes. Although Taylor's study differs substantially from our problem, he was the precursor of most of the studies listed below.

Frangolig & Fahien (1957) and Roley & Fahien (1960) studied carbon dioxide diffusive mass transfer in a vertical tube airflow. The carbon dioxide concentration was determined from the mixture thermal conductivity. They were able to obtain radial concentration profiles along the tube and highlighted the turbulent diffusion influence on the mixing and its homogeneity. However, these studies were limited to low Reynolds numbers (lower than 10,000), so the turbulent conditions were lower than those encountered in ventilation networks (greater than 10,000 and often up to 500,000).

Lynn et al. (1957) studied the mixing of coaxial streams of natural gas and air for Reynolds numbers of 44,000 and 79,000. This study aimed to determine the values of eddy diffusivity and viscosity by describing the natural gas spatial evolution in a duct and by proposing molar concentration radial profiles at different distances from injection. This study is rather interesting, especially the radial profiles, but coaxial mixing is rarely achieved in ventilation networks and the measurement technique was very intrusive.

Jordan (1960) evaluated mine ventilation flow rates using gaseous tracing. He used Shuttleworth's experimental data (unpublished) of tracer concentrations to validate an analytical model of the spatial distribution of the tracer concentration developed for different pipe geometries (rectangular and circular) and different tracer injection configurations (fixed and moving source point). Jordan showed radial concentration profiles at different distances from the central source. He was one of the first researchers to study the mixing length for source point injection and to try to decrease this length. However, Jordan's study remains essentially theoretical and he did not perform an experimental parametric study.

Evans (1967) was inspired by Jordan's work and proposed an experimental and analytical study in which he developed an analytical model describing the spatial turbulent diffusion of a tracer in a pipe flow. To validate this model, Evans performed an experimental setup for studying the tracer (Nigrosine) diffusion in water for Reynolds numbers ranging from 10,000 to 100,000. He measured many radial concentration profiles at different distances from the injection and evaluated the well-mixing length for each Reynolds number by considering that well-mixing was achieved at the distance from the injection where the minimum concentration was 99 percent of the maximum concentration. Evans also highlighted that the mixing length increased with the Reynolds number and proposed a model depending on the Reynolds number, the friction factor and the turbulent Schmidt number. Clayton (1968) proposed a similar approach and conducted a study on the Reynolds number's influence on the mixing length and tested different locations and different injection types. Clayton and Evans came to the same conclusion as regards the influence of the Reynolds number.

Quarmby & Anand (1969) carried out a similar study to those of Evans and Clayton using another tracer, nitrous oxide, in the airflow. The experimental results obtained were consistent with those of Evans, but Quarmby focused more on the turbulent diffusion rather than on the mixing length.

Several researchers have put forward experimental results associated with semi-empirical models or simulations. For instance, Ger & Holley (1974 and 1976) and Fitzgerald & Holley (1979) who were essentially interested in a single injection position (center or wall) and in the orientation of the injection (co-flow or crossflow). Ger was the first to use the variation coefficient parameter (COV) on a section. Based on their own experimental data, Gupta (1999), Anand et al. (2003) and Seo et al. (2006) have contributed to this field of research by proposing mixing length models depending on the variation coefficient.

It is noteworthy that the mixing length and more widely the turbulent diffusion represent an essential issue. Both have been the focus of experimental and numerical studies. However, these studies have mainly focused on cylindrical ducts and used intrusive measurement techniques that did not allow for several measurement points.

Our work aims at first to propose semi-analytical models to compute the well-mixing in different configurations of nuclear ventilation networks. These models can be applied in other industrial sectors for the design of building ventilation networks. Another aim is to evaluate the error committed on the measurement of the concentration when mixing length cannot be reached.

To develop the models and to validate the CFD codes needed to perform parametric studies, we developed an experimental device, described below, in order to measure the tracer concentration by using a non-intrusive laser diagnostic technique.

2 EXPERIMENTAL STUDY

2.1 Experimental setup

The experimental device was designed to be the most representative of nuclear ventilation networks. No standard configuration exists, but generally, the section is rectangular (above a maximum diameter due to obstruction reasons), the hydraulic diameter ranges from 0.1 m to 1 m, and the flow velocities range from 1.0 m.s^{-1} to 10 m.s^{-1} , corresponding to Reynolds numbers ranging from 10^4 to 10^6 .

Two duct geometries were chosen, circular and rectangular ones; the first one allows comparison of our experimental results with literature data (in particular Evans, 1967) and validation of an analytical model; the second one to study a more realistic case. In view of the subject of this article, only the results for the circular section are presented.

The complete geometry of the device is presented in Figure 1.

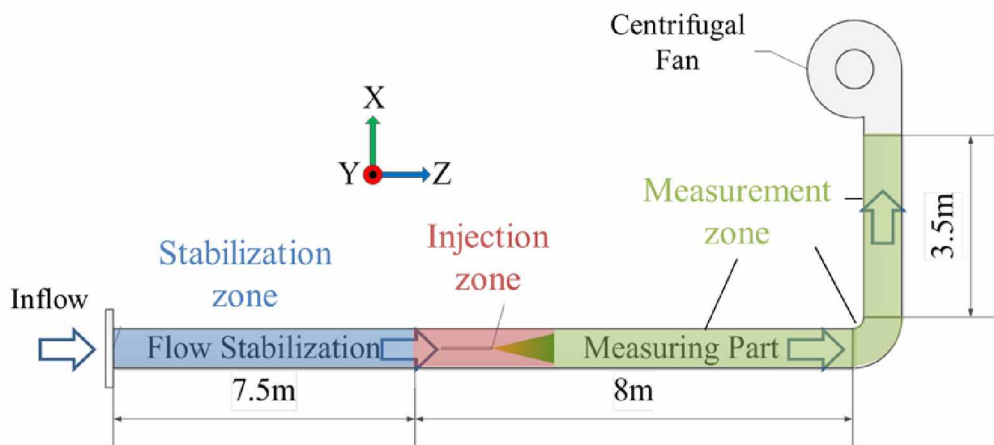


Figure 1: experimental device

The device is composed of three cylindrical sections with diameters of 0.2 m. The first one allowing the establishment of the flow is a 7.5 m straight pipe in PVC. The second one, in transparent material, is the injection zone of the seeded tracer. The last one, also in transparent material, is the working section. It includes a straight pipe of 8 m, then a 90° bend, and another straight pipe of 3.5 m until the centrifugal fan. This is where the tracer concentration measurement is performed using the laser method described in Section 2.2.

The internal duct airflow was achieved by the centrifugal fan providing a Reynolds number ranging from 10,000 to 250,000 inside the duct. At the duct entrance, a calibrated diaphragm allows control of the air flow rate and so the mean velocity which was also measured with a hot wire velocity probe. After the flow establishment section, the tracer injection was performed by an atomizer producing a thick smoke of oil droplets (DEHS for Di-Ethyl-Hexyl-Sebacat) with a diameter lower than 1 μm , ensuring that it is a good tracer of the flow (Stokes number of $5 \cdot 10^{-2}$), and a number concentration of around $10^6 \text{ \#} \cdot \text{cm}^{-3}$. The flow rate of the smoke was also calibrated and injected by a 5 mm diameter nozzle located at the centre of the pipe and according to local isokinetic conditions.

The concentration measurement method by means of laser diagnostics is detailed in the next section.

2.2 Measurement method

The tracer concentration measurement device was based on the light intensity of a laser beam (line), scattered by the particles passing through it, and recorded by a CCD camera, both located in the perpendicular axis to the flow (Figure 2). The laser was a He-Ne with 1 mW power stabilized at 0.2% and with a wavelength centered on 632 nm. The CCD camera had a resolution sensor of $1,628 \times 1,236$ pixels and a grayscale of 256 per pixel. It could acquire a maximum of 20 images per second. The device was located at the focal distance.

The entire system was implemented on a mobile carriage making it possible to move the laser-camera system to different locations along the working section without modifying the system configuration.

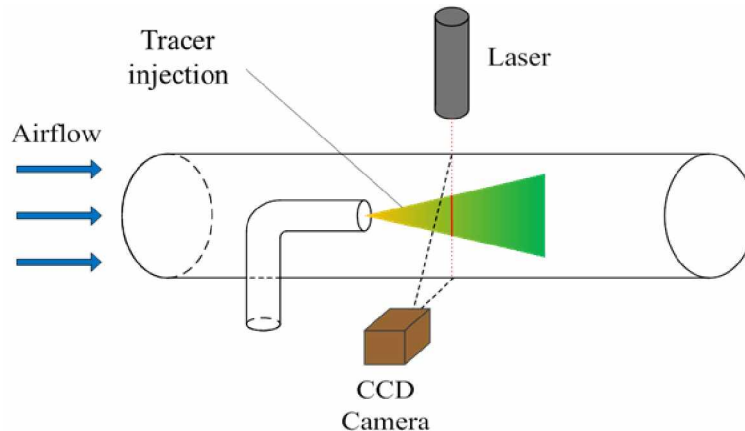


Figure 2: scheme of the measurement device principle

The light intensity emitted by the particles is acquired by a CCD camera and converted in gray levels per pixel. 300 images are necessary to be recorded in order to obtain an average image on the whole duct diameter. Then the average concentration is deduced from the average gray levels of this image. It can be noticed that, before each light intensity measurement, a background noise image was performed and systematically removed from the other acquired images.

Figure 3 presents an example of a signal acquired by the laser-camera system.

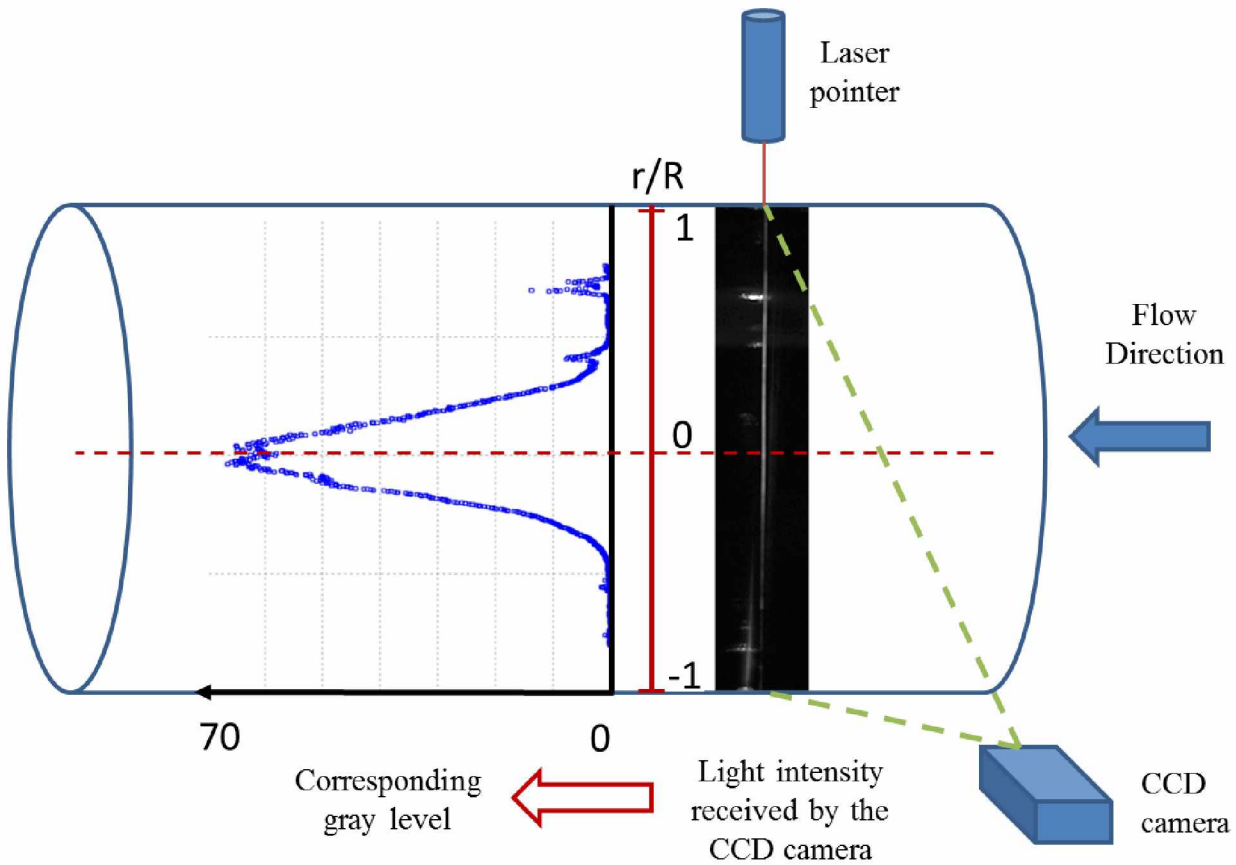


Figure 3: average image obtained at $z = 4 D$ from the injection and example of associated gray level radial profile ($Re = 50,000$; Axisymmetric and local isokinetic injection)

The conversion of a gray level profile to a concentration profile needs two steps. The first one is the usual image preprocessing allowing the pixel correction. Indeed, due to the cylindrical geometry of the duct and to the wide-angle-lens, chosen for approaching the CCD camera the closest to the duct and for measuring the tracer concentration on the entire diameter, the gray levels of the pixels are deformed and attenuated. These phenomena were evaluated thanks to a uniformly white light screen located inside the duct at the center (Figure 4).

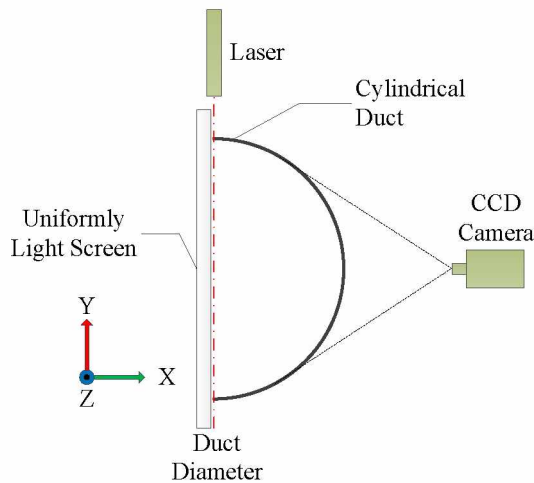


Figure 4 : location of the uniformly white screen in the cylinder

The first correction is the vignetting, which is the attenuation of the gray levels (Figure 5-a and b), revealed by a white image diffused by the screen.

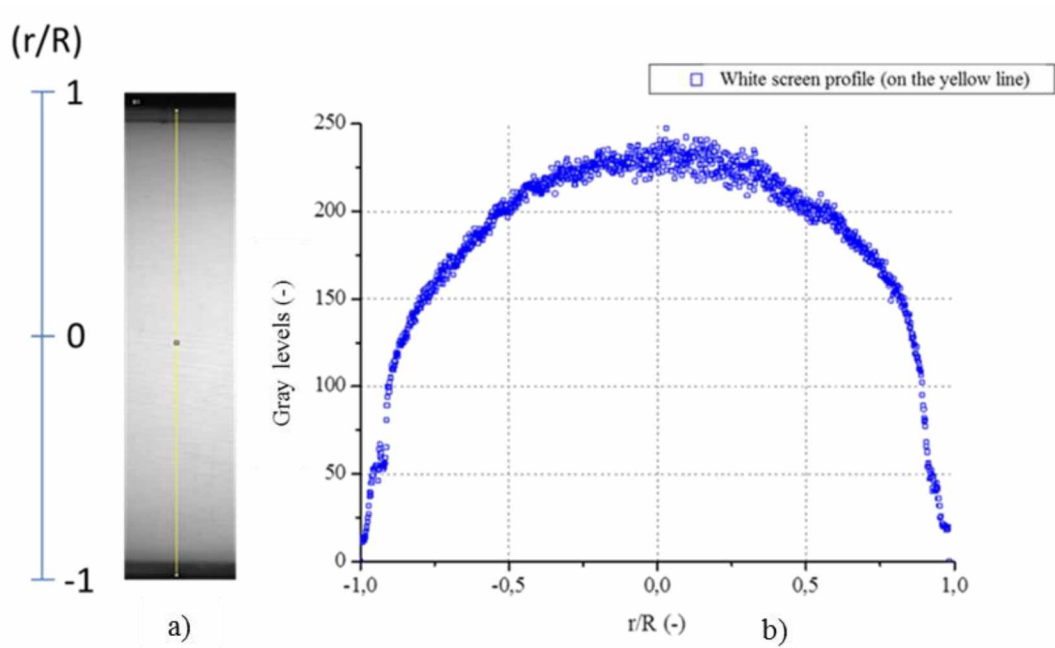


Figure 5 : a) reference image obtained in the duct ; b) grayscale profile obtained from the yellow path in the reference image

Then an image of checkered pattern, diffused by the screen, was used for straightening up the pixels (Figure 6).

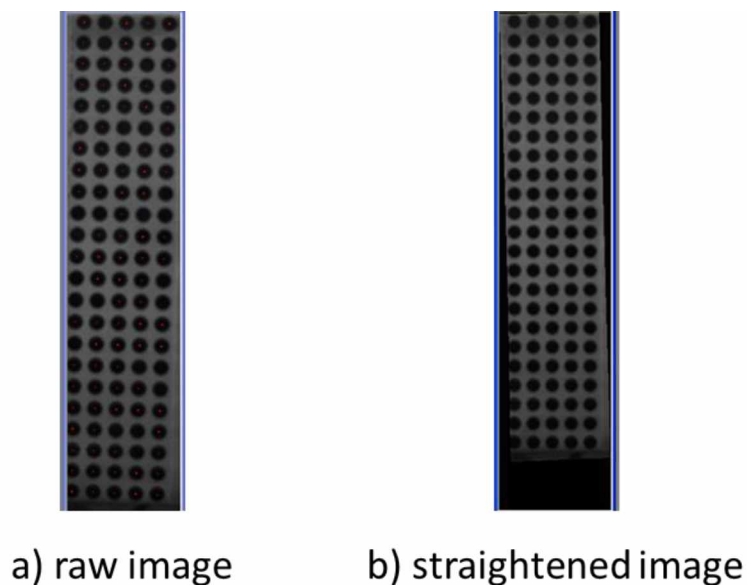


Figure 6 : example of straightened pixels obtained with the checkered pattern

During the measurements and due to the “patch” images approach, the results revealed an attenuation phenomenon of the average signal. This attenuation appears most of the time when the tracer concentration is close to the theoretical homogeneous concentration. In order to prove this phenomenon, two measurements were made with two different configurations of the laser-camera system at 10 D from the injection point: Figure 7-a) presents the reference configuration of the system and in Figure 7-b) the device remains vertical but the direction of the laser beam is inverted.

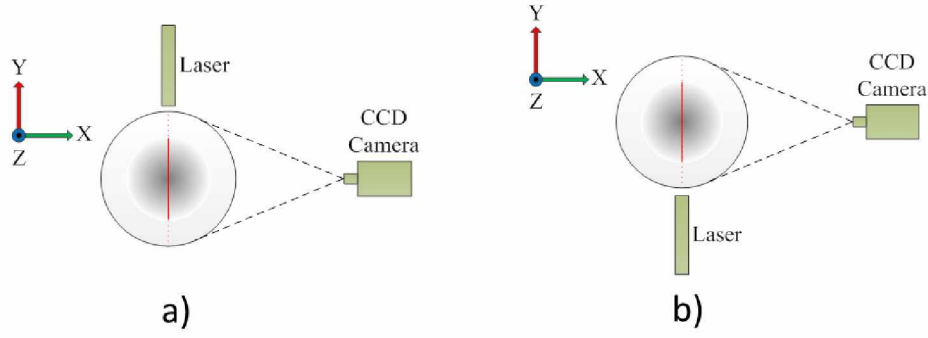


Figure 7 : a) reference configuration of the laser device; b) inverse configuration of the laser device

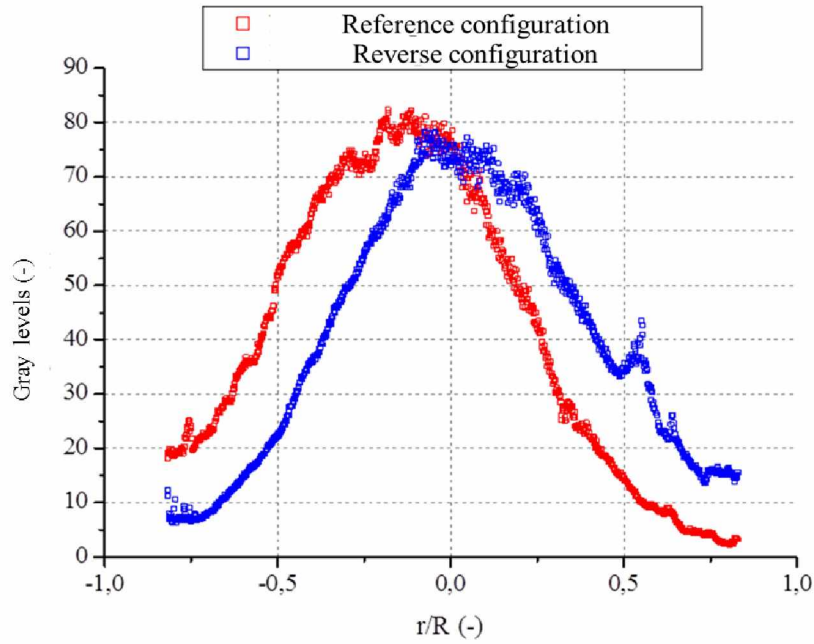


Figure 8 : comparison of the gray levels between the normal and the inverse configurations versus the radial distribution divided by the duct radius measured at 10 D from the injection (Re = 50,000 ; Axisymmetric and local isokinetic injection)

Figure 8 shows the results obtained with both laser configurations presented in Figure 7 : there is a symmetrical attenuation that can be explained by the extinction law of Beer-Lambert (1):

$$I_a(i) = I_i \cdot e^{-(\beta \cdot i)} \quad (1)$$

where I_a is the attenuated signal intensity, I_i is the incident signal intensity, β is the attenuation coefficient (m^{-1}) and i the distance from the inlet point of the laser beam in the duct (m).

The difficulty is to define the value of β that depends on the concentration distribution crossed by the Laser beam whereas this distribution concentration is unknown. In order to estimate this coefficient, concentration measurements were performed for different known air flowrates in duct and for an injection flowrate fixed, at a distance enough important to ensure a homogeneous concentration in the entire section (around 30 D downstream of the injection). Then, coefficients β were calculated thanks to the equation (2) and a range is comprised between $4 \cdot 10^{-4} m^{-1}$ and $10^{-3} m^{-1}$.

$$\beta = \frac{1}{i} \ln \left(\frac{I_i}{I_a} \right) \quad (2)$$

Taking into account the low value of this coefficient, a strong assumption was made to use β as a constant. The idea is to straighten the gray level profiles in order to become symmetrical. Figure 9 presents a straightened signal measured at 30 D downstream of the injection with this constant coefficient. The result shows that the constant assumption is quite valid in the case of an axisymmetric injection.

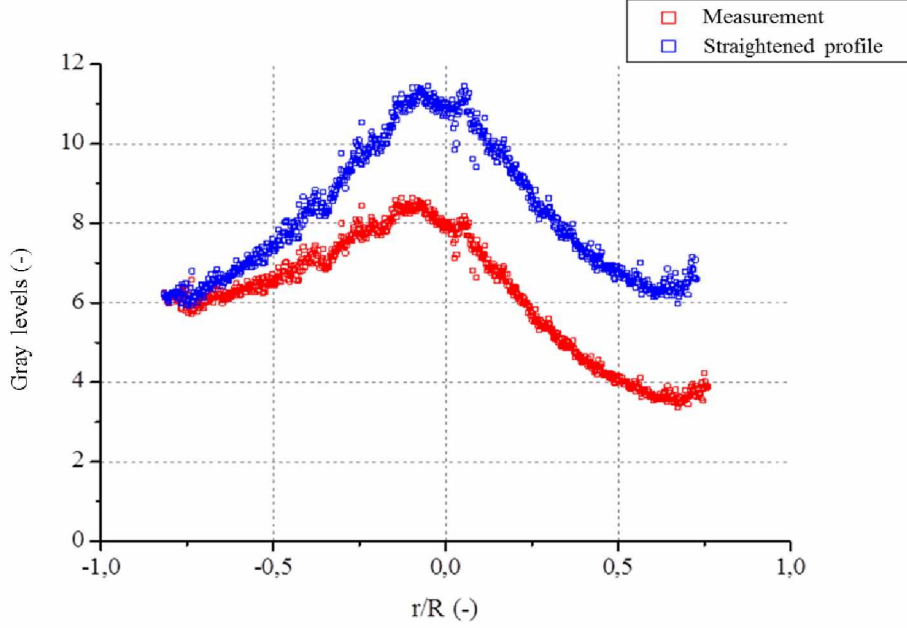


Figure 9: example of gray level radial profile straightened with a constant coefficient measured at 30 D downstream of the injection ($Re = 50,000$; Asymmetrical and local isokinetic injection)

During the acquisition, the camera gain was unitary and the camera's diaphragm was open at its maximum. The goal of the measurement was to obtain an average image of light intensity on the whole duct diameter. Once the system was calibrated, the average field of the tracer concentration could be deduced from this image.

2.3 Correlation between gray levels and concentration

The image post-processing is the actual conversion of the gray levels to concentration. This technique is developed in order to measure the tracer concentration the nearest of the homogenous concentration, while the smoke atomizer does not permit to know precisely the injection concentration. So, it was decided to use relative value of the concentration considering the gray level of the injection profile as a reference (3).

$$\frac{C}{C_{max}}(r/R, z/D) = \frac{GL(r/R, z/D)}{GL_{max}} \quad (3)$$

where C is the local concentration (kg.m^{-3}), C_{max} is the injection concentration (kg.m^{-3}), GL is the local measured gray level (-), GL_{max} is the maximal gray level (-), r/R is the radial distance from the duct center divided by the duct radius and z/D (-) is the distance from the injection divided by the duct diameter.

The maximal gray level is defined as the gray value measured below the light saturation. Thus, the shutter time of the CCD camera is adjusted in order to measure the maximum gray value below 250 (generally). Then, a maximum threshold profile crenellated is averaged to get GL_{max} from the initial profile at the injection (Figure 10). This calibration was conducted in-situ for each duct geometry and with the same laser-camera setup as for the concentration measurements.

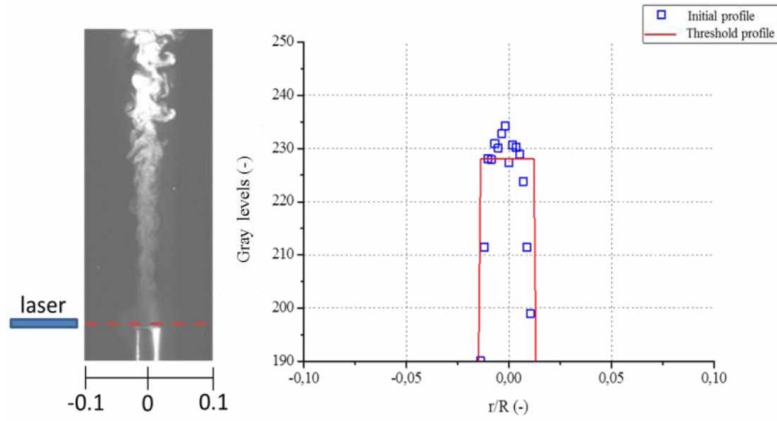


Figure 10: example of threshold radial profile obtained at the injection ($Re = 50,000$; Axisymmetric and local isokinetic injection)

After this step, the homogenous concentration C_H is introduced in the equation (4), by considering that $C_H = C_{max} \cdot \frac{q_{inj}}{Q_f}$ (where $\frac{q_{inj}}{Q_f}$ represents the dilution rate):

$$\frac{C}{C_H}(r/R, z/D) = \frac{GL(r/R, z/D)}{GL_{max}} \cdot \frac{Q_f}{q_{inj}} \quad (4)$$

where Q_f is the air flowrate in duct ($kg \cdot s^{-1}$), q_{inj} is the injection flowrate ($kg \cdot s^{-1}$), both parameters fixed and known for each tests, and C_H is the homogenous concentration ($kg \cdot m^{-3}$).

This correlation is based on the assumption that the concentration and the gray levels have a linear behavior, that which has been verified and shown in the further section in this paper. Then, the most important part of the image post-processing is the step called “patch”. In fact, the problem comes from the low values of gray levels available with this 8-bit CCD camera to observe the lowest concentration far from the injection. This difficulty was overcome using the shutter time of the CCD camera: when the shutter time is increased, the signal recorded by the camera is amplified. The next paragraph tries to demonstrate that a link exists between two profiles of gray levels obtained in one measurement point and for two different shutter times.

Figure 11 presents two curves of gray levels measured for different shutter times at 1.5D from the injection (black and blue). The red and green curves are obtained respectively by multiplying and dividing the previous profiles by a coefficient, called gain, defined by the value of the ratio between the two values of shutter times. It aims at ensuring that this gain does not alter the real signal.

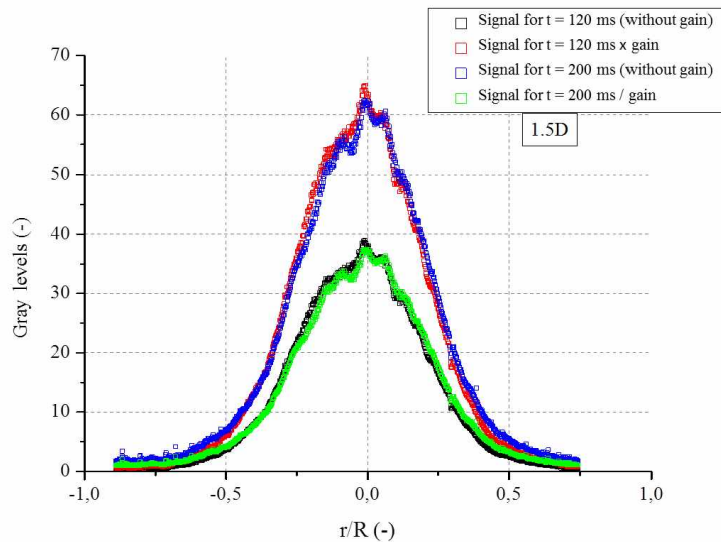


Figure 11: example of the influence of the shutter time on the gray levels profile ($Re = 50,000$; Axisymmetric and local isokinetic injection)

There is a good accuracy between the results measured with a given shutter time and another one modified by this gain at the same measurement point. This important result shows that it is possible to raise the gray levels when the light intensity is too low for the CCD camera sensor, by applying a gain without losing information. This technique, sometimes called “patch”, allows the switch of reference concentration along the duct when the concentration ratio is too low. For each test performed in this study, five new references were required to measure the lowest concentration for the whole duct.

There are many steps from the gray levels to the distribution of the concentration and all these calculations may generate few estimation errors. Three main sources of uncertainty are noted: the corrections of the gray levels (deformation, vignetting, and attenuation), the evaluation of the threshold profile at the injection, and the air and injection flowrates.

Thus, it was decided to estimate the relative uncertainty of the relative concentration from the equation (5).

$$\frac{u(c/c_H)}{c/c_H} = \sqrt{\left[\frac{u(GL)}{GL}\right]^2 + \left[\frac{u(GL_{\max})}{GL_{\max}}\right]^2 + \left[\frac{u(Q_f)}{Q_f}\right]^2 + \left[\frac{u(q_{inj})}{q_{inj}}\right]^2} \quad (5)$$

This approach allows the evaluation of the laser technique uncertainty; then the results show that the maximal value reaches 15%.

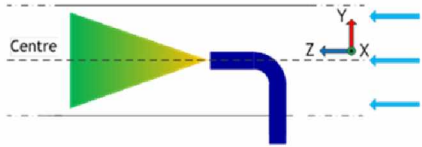
It can be noticed that a validation of this technique taking account this uncertainty calculation was performed with a classical gas tracing technique allowing to ensure a good confidence for this technique.

2.4 Experimental results

This section presents the results obtained on the experimental device for the duct with a circular section.

Considering the capacity of the device and the characteristics of nuclear ventilation networks, the following test grid (Table 1) was studied.

Table 1: test grid

Re (-)	Injection	
	Position	Velocity (m.s ⁻¹)
3.5x10 ⁴		U _{inj} = U _{max} = 3.4 m/s
5.0x10 ⁴		U _{inj} = U _{max} = 4.8 m/s
1.0x10 ⁵		U _{inj} = U _{max} = 9.5 m/s

In this test grid, three Reynolds numbers ranging from 35,000 to 100,000 were studied. These numbers were determined by the fan capacity. The injection velocity was equal to the maximal velocity of the flow and the injection orientation was in co-flow.

2.4.1 Reference test

The test with a Reynolds number of 50,000 served as the reference test, comparable to that of Evans (1967) which used a circular pipe with a diameter of 0.15 m. Based on this reference configuration, the Reynolds number was subsequently modified.

The measurement points were located at 4, 7, 10, 20 and 30 diameters downstream of the injection point, chosen as the reference concentration C_H. Each test was reproduced three times for calculating an average concentration profile.

Figure 12 shows the radial evolutions of the relative concentration C/C_H according to r^+ the radial position divided by the duct radius. These curves are truncated close to the duct wall because of the laser beam reflection on the wall.

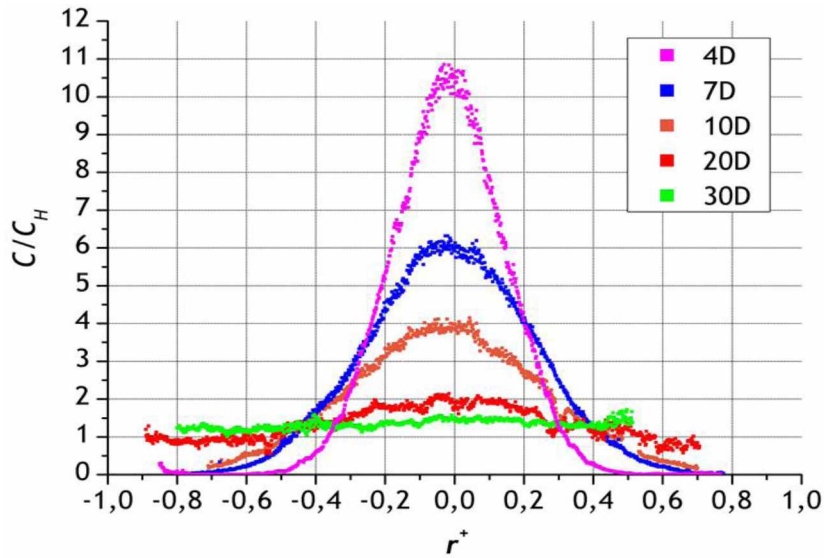


Figure 12: relative concentration radial profiles (Re = 50,000)

The profiles in Figure 12 seem to follow a Gaussian form with maximum concentrations in the center of the duct. The profiles are symmetric relative to the center of the duct and become flat when the tracer is mixed and moves away from the injection.

The measurement points located on the axis of the duct ($r^+ = 0$) were then compared to the measurement points of Evans (1967) in the same configuration. Figure 13 presents the evolution of the relative concentration C/C_H according to the distance from the injection point (z) normalized by the duct diameter (D).

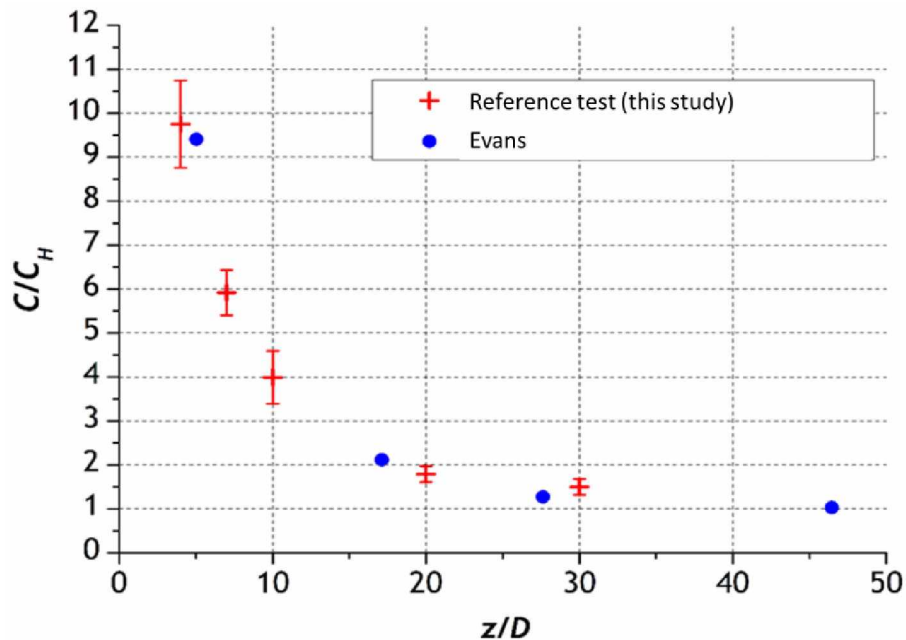


Figure 13: concentration axial profile for reference test compared to Evans test (Re = 50,000)

The comparison between the experimental results and those of Evans shows a good agreement and confirms the validity of the measurement method used. A slight gap can be observed between the two methods at 30 diameters. This gap is difficult to analyse because Evans, like most of the identified researchers, did not provide measurement uncertainties.

2.4.2 Influence of the Reynolds number

As mentioned previously, two other Reynolds numbers, 35,000 and 100,000, were also studied. The results obtained are presented and compared to the reference test in Figure 14.

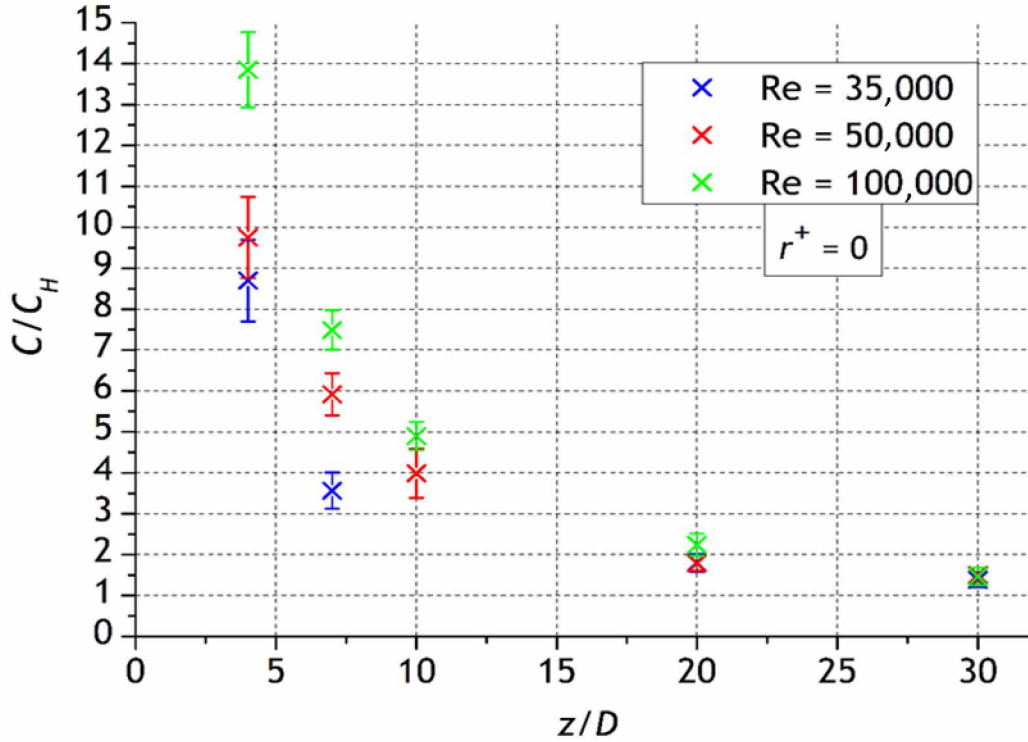


Figure 14: concentration axial profiles for Reynolds numbers of 35,000 and 100,000 compared to the reference test (50,000)

Figure 14 shows that the different profiles all tend toward a homogeneous concentration $C/C_H = 1$ for a distance z greater than 30 diameters. It highlights also that the more the Reynolds number increases, the greater the importance of the mixing length, that is not necessarily obvious as it could seem more consistent that higher Reynolds numbers will entail a more perturbed flow and more homogeneous mixing.

This trend was also observed by several authors such as Roley (1960), Evans (1967) or Quarmby (1969).

In a first approach, this trend does not seem intuitive, considering that the higher the Reynolds number, the more turbulent the flow and the better the tracer mixing is; however, by comparing convection due to the flow and radial turbulent diffusion and by introducing a dimensionless turbulent Peclet number (see section 3.1), it can be highlighted that this latter is depending on Re^n with $n > 0$. Hence, when Reynolds number increases, turbulent Peclet number too, so convection is stronger than radial diffusion and the mixing length is greater.

This explanation will be verified in the section 3.2.

3 ANALYTICAL MODEL DEVELOPMENT

3.1 Spatial evolution of the tracer concentration

The first step of the development of our analytical model is to write the advection-diffusion equation for a passive scalar.

$$\vec{\nabla} \cdot (\vec{u}C) = \vec{\nabla} \cdot [(D_m + D_t) \cdot \vec{\nabla}(C)] \quad (6)$$

In the equation (6), the term on the left represents the advection and the term on the right represents the diffusion.

In order to solve this equation, some assumptions are needed and were also applied by the most of authors which developed this kind of model (Evans, 1967; Quarmby, 1969; Ger, 1974). The molecular diffusion coefficient D_m is negligible compared to the turbulent diffusion coefficient D_t .

Taking into account the continuity equation $\vec{\nabla} \cdot (\vec{u}) = 0$, the equation (6) can be simplified:

$$\vec{u} \vec{\nabla} \cdot (C) = \vec{\nabla} \cdot [(D_t) \cdot \vec{\nabla}(C)] \quad (7)$$

As the shape of the duct is cylindrical, it seems relevant to use cylindrical coordinates (Figure 15).

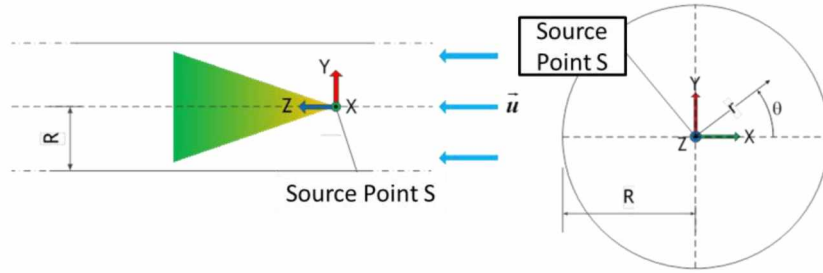


Figure 15: problem schematization with cylindrical coordinates

The conversion of the equation (7) with the cylindrical coordinates, following the scheme in Figure 15, is given below:

$$u_z \frac{\partial C}{\partial z} = \frac{1}{r} \frac{\partial}{\partial r} \left(r D_t \frac{\partial C}{\partial r} \right) + \frac{1}{r^2} \frac{\partial}{\partial \theta} \left(D_t \frac{\partial C}{\partial \theta} \right) + \frac{\partial}{\partial z} \left(D_t \frac{\partial C}{\partial z} \right) \quad (8)$$

This equation can be simplified, considering that the longitudinal velocity u_z is sufficiently high for neglecting the longitudinal diffusion term:

$$u_z \frac{\partial C}{\partial z} \gg \frac{\partial}{\partial z} \left(D_t \frac{\partial C}{\partial z} \right) \quad (9)$$

By considering the revolution symmetry, the angular component can be also neglected.

Hence, the equation (8) becomes:

$$u_z \frac{\partial C}{\partial z} = \frac{1}{r} \frac{\partial}{\partial r} \left(r D_t \frac{\partial C}{\partial r} \right) \quad (10)$$

To solve this equation, a variable separation method is used. The constant parameters must be identified and grouped together in order to reveal non-dimensional parameters. By considering the longitudinal velocity u_z as a constant equal to the flow velocity U_d and the radial diffusion coefficient D_t as a constant (due to the

revolution symmetry) and by dividing the coordinates r and z by the duct radius R , one reveals the turbulent Peclet number defined as $Pe_t = \frac{RU_d}{D_t}$, and obtains the following equation:

$$Pe_t \frac{\partial C}{\partial z^+} = \frac{1}{r^+} \frac{\partial}{\partial r^+} \left(r^+ \frac{\partial C}{\partial r^+} \right) \quad (11)$$

with $r^+ = \frac{r}{R}$ and $z^+ = \frac{z}{R}$

It can then be assumed that the solution is a linear combination of elementary solutions with separated variables that are defined by:

$$C(z^+, r^+) = \sum_n \sum_p A_n(z^+) B_p(r^+) \quad (12)$$

All the elementary solutions must satisfy the equation (11), which, by replacing $C(z^+, r^+)$ by its expression, becomes:

$$Pe_t \frac{A'_n(z^+)}{A_n(z^+)} = \frac{1}{r^+ B_p(r^+)} \frac{d}{dr^+} \left(r^+ B'_p(r^+) \right) \quad (13)$$

Where $A'_n(z^+)$ and $B'_p(r^+)$ are the first derivatives respectively of $A_n(z^+)$ and $B_p(r^+)$.

This equality is only possible if each side of the equation is equal to an arbitrary constant noted $-a_{np}$.

$$\frac{A'_n(z^+)}{A_n(z^+)} = -\frac{a_{np}}{Pe_t} \quad (14)$$

$$\frac{1}{r^+ B_p(r^+)} \frac{d}{dr^+} \left(r^+ B'_p(r^+) \right) = -a_{np} \quad (15)$$

This variable separation allows writing the following equation system:

$$A'_n(z^+) + \frac{a_{np}}{Pe_t} A_n(z^+) = 0 \quad (16)$$

$$(r^+)^2 B''_p(r^+) + r^+ B'_p(r^+) + a_{np} (r^+)^2 B_p(r^+) = 0 \quad (17)$$

The first equation is a first order linear equation that is quite easy to solve. The solutions for the second equation, known as a Bessel equation, are known (Sturm-Liouville problem).

Finally, by integrating the solution of this equation system with the equation (12), the latter becomes:

$$\frac{C}{C_H}(z^+, r^+) = 1 + \sum_{n=1}^{\infty} \exp\left(-\frac{a_n}{Pe_t} z^+\right) \frac{J_0(r^+ \sqrt{a_n})}{[J_0(\sqrt{a_n})]^2} \quad (18)$$

where C_H is the homogeneous concentration, J_0 is the 0 order Bessel function, and a_n is the integration constant that can be calculated by the way of initial conditions and of the specificity of the Bessel functions:

$$J_1(\sqrt{a_n}) = 0 \text{ and } a_0 = 0 \quad (19)$$

where J_1 is the 1st order Bessel function.

In this expression, all the parameters are known except Pe_t because of the radial turbulent diffusion D_t that is expressed by:

$$D_t = \frac{\nu_t}{Sc_t} \quad (20)$$

The turbulent Schmidt number Sc_t is generally equal to 1 for Reynolds numbers over 50,000 (Evans, 1967), so the eddy viscosity ν_t must be determined. The next section proposes to choose an eddy viscosity profile model among those found in the literature and to average it by integration along the duct radius:

$$D_t = \frac{\overline{\nu_t}}{Sc_t} = \frac{1}{Sc_t} \int_0^1 \nu_t(r^+) dr^+ \quad (21)$$

3.2 Eddy viscosity modelling

This section aims to define a model to describe the radial profile of eddy viscosity in a duct.

Various authors, for instance Reichardt (1951), Van Driest (1956), Mizushima (1969) and Guo (2003), have proposed this type of model with different validity ranges for r^+ (Table 2).

Table 2: eddy viscosity models from the literature

Authors	Expressions	Range of validity for r^+
Reichardt (1951)	$\frac{\nu_t}{RUf} = \frac{\kappa}{6} \left[1 - (r^+)^2 \right] \cdot \left[1 + 2(r^+)^2 \right]$	$0 \leq r^+ \leq 0.995$
Van Driest (1956)	$\frac{\nu_t}{RUf} = 2\kappa(1 - r^+) (r^+)^{1/2}$	$0 \leq r^+ \leq 0.97$
Mizushima (1969)	$\frac{\nu_t}{RUf} = 0,07$	$0 \leq r^+ \leq 0.77$
Guo (2003)	$\frac{\nu_t}{RUf} = \frac{r^+}{\frac{\sqrt{3}e}{2} \left(\frac{1}{1-r^+} - (1-r^+)^2 \right) + \pi \sin(\pi(1-r^+))}$	N/A

Other authors, for instance Nunner (1956), Laufer (1954), Reichardt (1951) and Quarmby (1969), have proposed experimental data of eddy viscosity profiles in ducts.

In order to compare the models with their experimental data, the eddy viscosity ν_t is divided by the friction velocity U_f and the duct radius R .

This comparison is presented in Figure 16, making it possible to choose the most relevant eddy viscosity model for implementation in our analytical model described in Section 3.1.

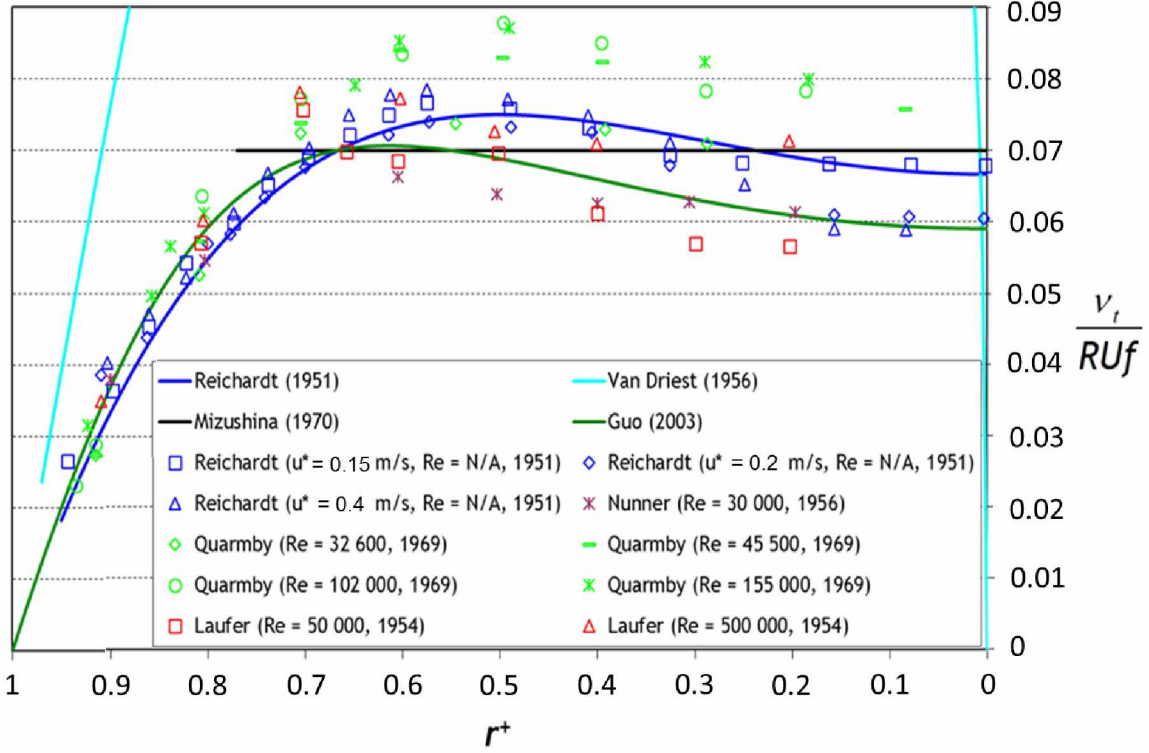


Figure 16: comparison between eddy viscosity models and experimental data

Considering that Guo's model was developed on the basis of Reichardt's, Laufer's and Nunner's experimental data, whereas Reichardt's model was fitted only on his own experimental data, Guo's model was chosen, assuming it is more representative. Hence, the expression of the radial diffusion coefficient D_t , integrating Guo's model averaged on the duct radius, becomes:

$$D_t = \frac{0.058 R U_f}{Sc_t} \text{ with } U_f = U_d \sqrt{\frac{\lambda}{8}} \quad (22)$$

Finally, this coefficient can be integrated into the concentration model from the equation (18):

$$\frac{C}{C_H}(z^+, r^+) = 1 + \sum_{n=1}^{\infty} \exp\left(-\frac{0.058}{Sc_t} a_n \sqrt{\frac{\lambda}{8}} z^+\right) \frac{J_0(r^+ \sqrt{a_n})}{[J_0(\sqrt{a_n})]^2} \quad (23)$$

This model is especially interesting due to its relative simplicity and its need for substantially less data than the Evan's model which needs an initial concentration profile; the coefficient a_n can be calculated by using the initial conditions of the equation (19) while the friction coefficient λ depends on the Reynolds number and the wall roughness (Colebrook [1939]). In our case, as the duct is smooth, the friction factor was calculated by the Blasius correlation (19):

$$\lambda = 0.316 Re^{-0.25} \quad (24)$$

Knowing all the parameters of the turbulent Peclet number, the latter can be expressed according to the Reynolds number:

$$Pe_t = \frac{Sc_t}{0.058} \sqrt{\frac{8}{\lambda}} = \frac{Sc_t}{0.058} \sqrt{\frac{8}{0.316} Re^{0.25}} \propto Re^n \text{ with } n = 0.125 \quad (25)$$

This last equation allows the confirmation that Pe_t is proportional to Re^n , as mentioned in section 2.4.2, and that the mixing length will increase with the Reynolds number.

4 ANALYTICAL MODEL VALIDATION

This section aims to validate the analytical model developed by comparing it to the experimental data acquired on the experimental device described in Section 2.

A first comparison is performed for axial profiles and different Reynolds numbers.

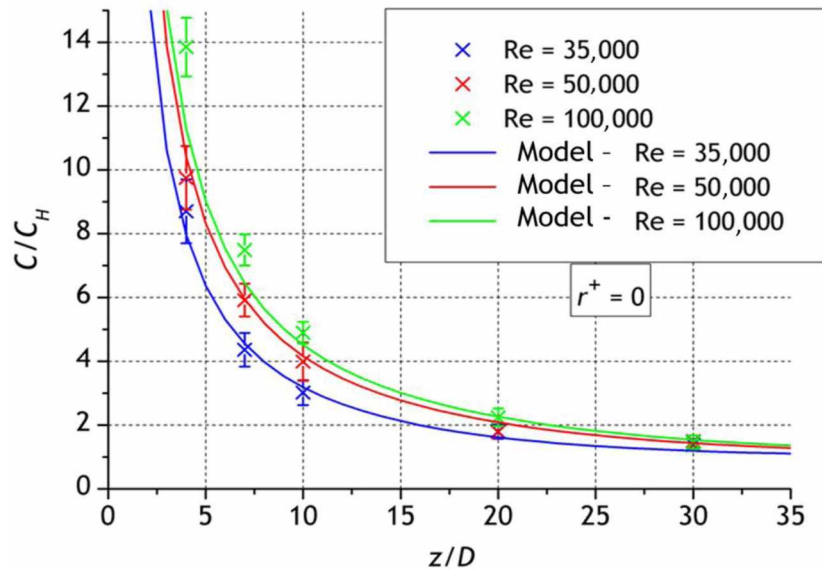


Figure 17: experimental axial profiles of dimensionless concentration compared to the analytical model for different Reynolds numbers

The comparison presented in Figure 17 shows a good agreement between the model and the experimental data. The evolution is well reproduced; taking into account the experimental uncertainties, the model calculates quite precisely the concentration values at different distances from the injection.

A first remark is that the model confirms the concentration evolution with the Reynolds number; the lower the Reynolds number is, the more homogeneous the mixing becomes.

On the other hand, notice that the mixing becomes truly homogeneous after around 25 D. For example, for a duct with a 20 cm diameter, the needed length is equal to 5 m.

A comparison is also done for radial profiles at different distances from the tracer injection and for the three studied Reynolds numbers. The aim is to evaluate the radial dispersion modelling of the tracer.

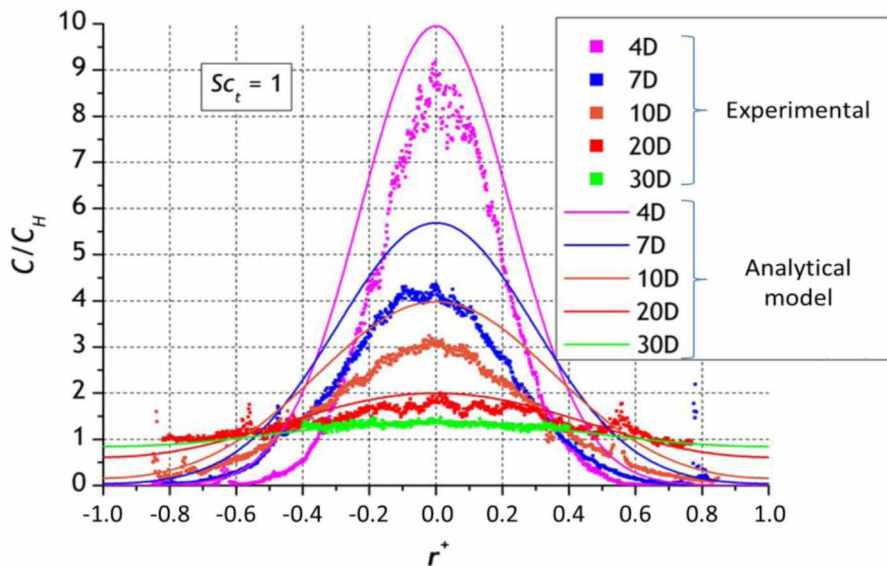


Figure 18: experimental radial profiles of dimensionless concentration at different distances from the injection compared to the analytical model ($Re = 35,000 - Sc_t = 1$)

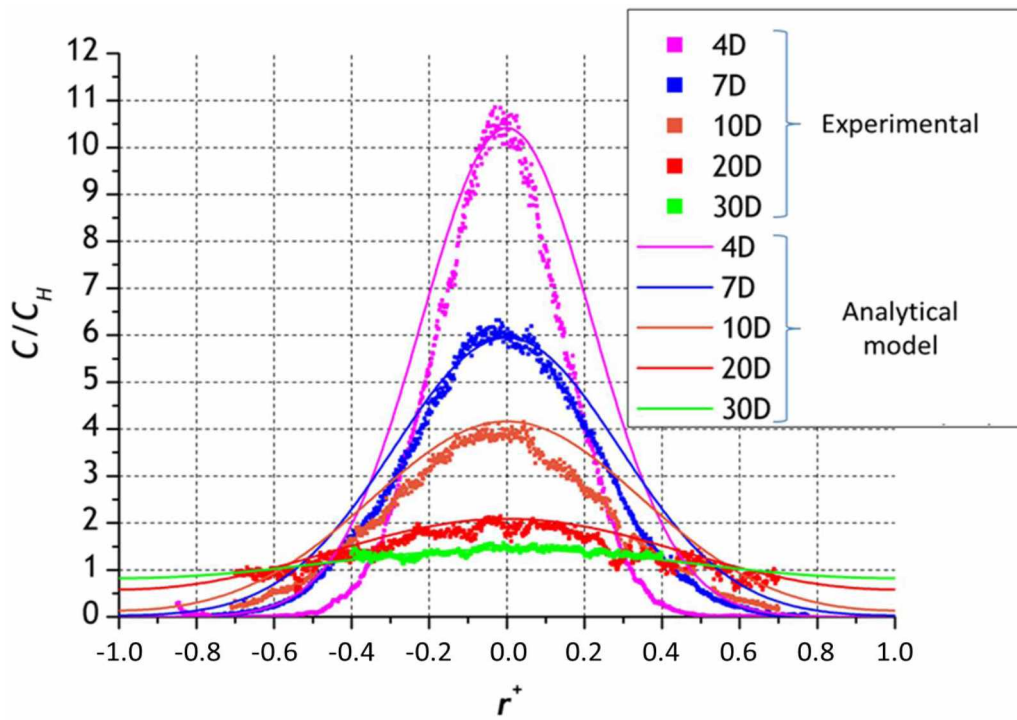


Figure 19: experimental radial profiles of dimensionless concentration at different distances from the injection compared to the analytical model ($Re = 50,000 - Sc_t = 1$)

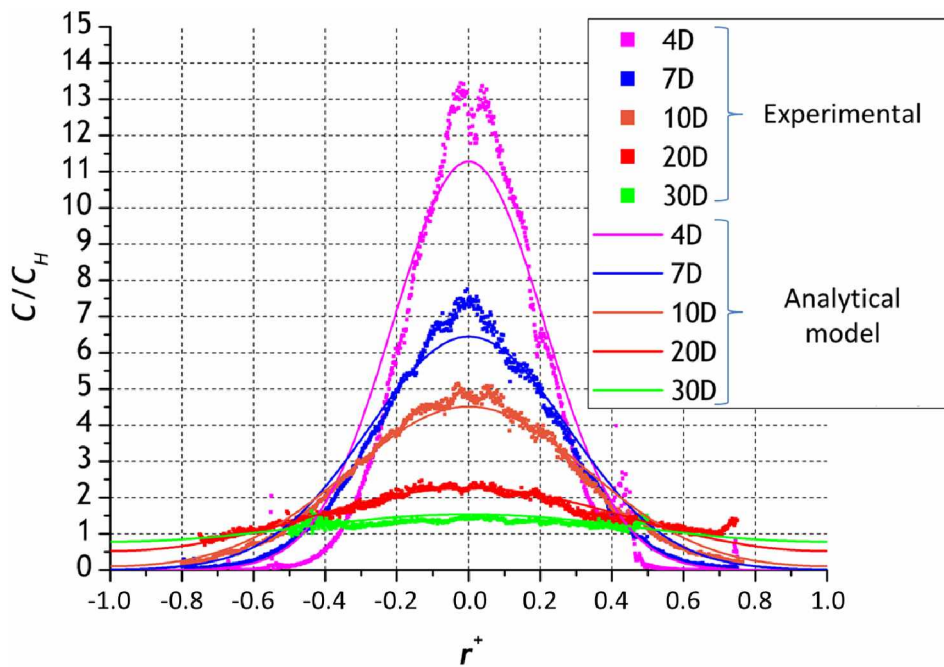


Figure 20: experimental radial profiles of dimensionless concentration at different distances from the injection compared to the analytical model ($Re = 100,000 - Sc_t = 1$)

The model results presented in Figure 18, Figure 19 and Figure 20 are in quite good agreement with the experimental data. The experimental Gaussian evolution is well described by the analytical model. However, significant differences with the experimental data are highlighted for the lowest Reynolds number ($Re = 35,000$).

The explanation that can be proposed, according to Evan's article, is that the turbulent Schmidt number can be below 1 for Reynolds numbers below 50,000. Additional lower values of turbulent Schmidt number were tested for the Reynolds number of 35,000; a value of 0.8 allowed to better reproduce the experimental results (Figure 21).

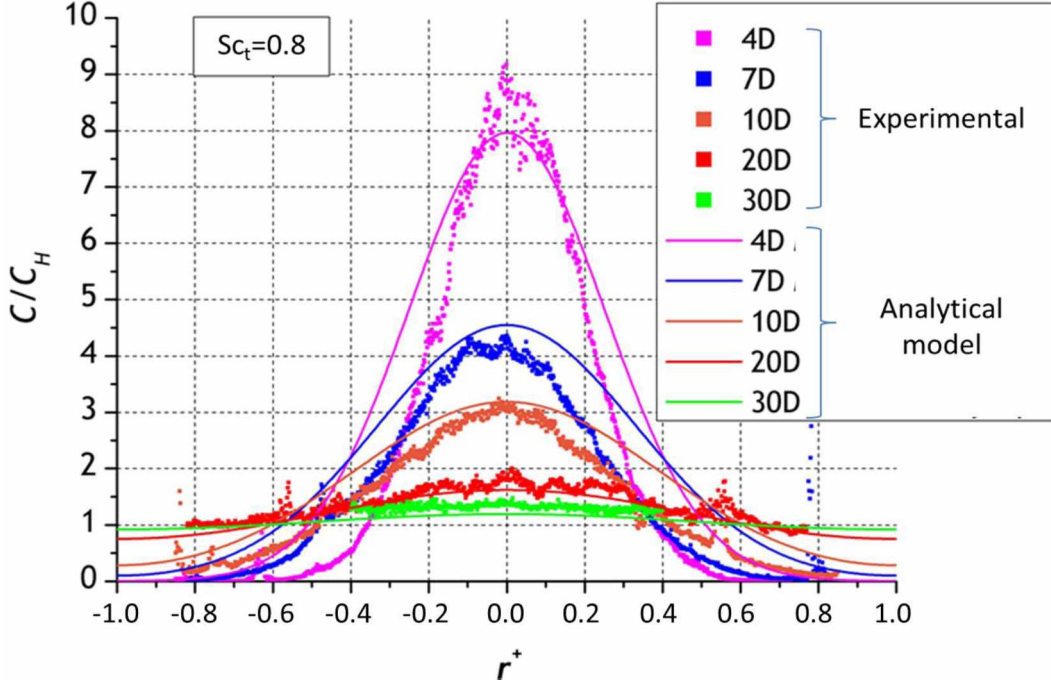


Figure 21: experimental radial profiles of dimensionless concentration at different distances from the injection compared to the analytical model ($Re = 35,000 - Sc_t = 0.8$)

5 MODEL APPLICATION IN INDUSTRIAL CONTEXT

In the previous sections, an analytical model of tracer spatial dispersion has been presented in its integral form. This model is in quite good agreement with experimental data reported here and also with data from Evans (1967). However, its use is not very practical, especially for industrial applications. Indeed, neither the determination of the Bessel function roots, nor the implementation of the model is easy.

A model simplification is therefore needed in order to easily apply it in industrial situations.

In this model, the major difficulty is the Bessel function sum and the root determination. A first approximation is to reduce the number of terms in the sum in order to only keep one term. This simplification is proposed in the equation (26), in which $z^+ = \frac{z}{R}$ is replaced by $z^* = \frac{z}{D}$, where D is the duct diameter.

$$\frac{C}{C_H}(z^*, r^+) = 1 + \exp\left(-2 \times \frac{0.058}{Sc_t} a_1 \sqrt{\frac{\lambda}{8}} z^*\right) \frac{J_0(r^+ \sqrt{a_1})}{[J_0(\sqrt{a_1})]^2} \quad (26)$$

Where a_1 is the square of the first nonzero root of the 1st order Bessel function J_1 and is equal to 14.682.

A comparison between the model with n terms and the one with one term is presented in Figure 22.

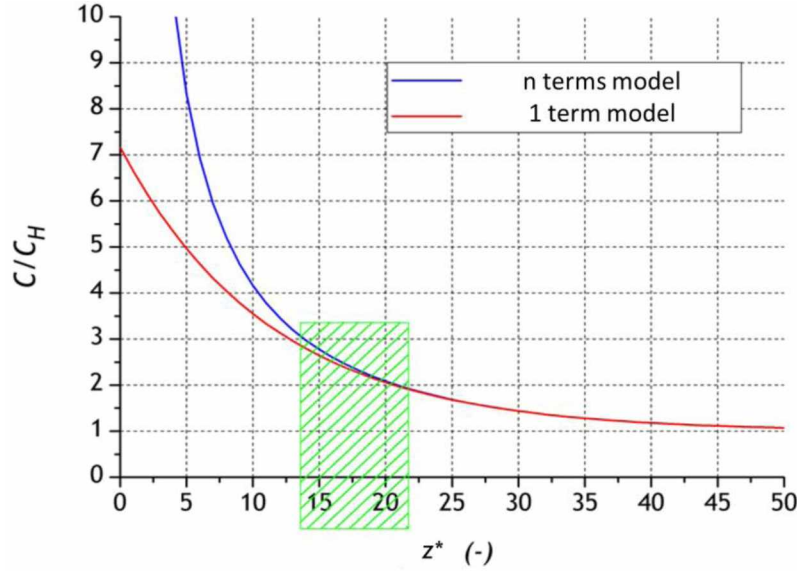


Figure 22: comparison between the n terms model and the one term model

Figure 22 clearly shows that after $z^* = 15$, both models meet and the one term model can be used in place of the n terms model. This makes it possible both to greatly simplify the analytical model and to invert it, unlike the n terms model; this inversion is of great interest for industrial applications.

Indeed, in ventilation networks, filters are disposed at the network outlets in order to retain potential hazardous materials which could be released. To ensure filter efficiency, periodic tests must be performed using the particle tracing technique. This technique consists in injecting a particle tracer, widely upstream of the filter, and to sample the particle concentration just upstream and downstream close to the filter. The ratio between both concentrations allows calculation of filter efficiency. However, the local samples must be representative of the concentration in the whole section and the concentration must therefore be homogeneous. This is why a sufficient duct length, called “Well Mixing Length”, is needed between the injection and the sample points. By using our analytical model, it becomes possible to determine this length by reversing it.

The model developed here allows calculation of a local relative concentration. In the present case, information on the whole section of the duct is more interesting to ensure the homogeneity of the concentration. A variation coefficient COV_c is therefore more appropriate. It is defined by:

$COV_c = \sqrt{\frac{1}{S} \int \left(\frac{c}{c_H} - 1\right)^2 dS}$ and by integrating the equation (26) into it, this expression becomes:

$$COV_c(z^*) = \frac{\sqrt{2}}{[J_0(\sqrt{a_1})]^2} \exp\left(-\frac{1.175}{Sc_t} \sqrt{\frac{\lambda}{8}} z^*\right) \sqrt{\int_0^1 r^+ J_0(r^+ \sqrt{a_1}) dr^+} \quad (27)$$

Once the integral is calculated numerically ($\int_0^1 r^+ J_0(r^+ \sqrt{a_1}) dr^+ = 0.0812$) and the pre-factor is replaced by its value 8.718, the equation (27) becomes the equation (22):

$$COV_c(z^*) = 2.48 \cdot \exp\left(-\frac{1.175}{Sc_t} \sqrt{\frac{\lambda}{8}} z^*\right) \quad (28)$$

The equation (22) can then be inverted and $z^* = \frac{L}{D}$ can be expressed as a function of COV_c :

$$z^* = \frac{L}{D} = 0.58 \cdot Sc_t \sqrt{\frac{8}{\lambda}} \cdot \ln\left(\frac{248}{COV_c(\%)}\right) \quad (29)$$

This expression is now compared to that of Ger & Holley (1976), who developed a similar model (30):

$$z^* = \frac{L}{D} = 6.91 \cdot \log\left(\frac{248}{COV_c(\%)}\right) \cdot Re^{0.104} \quad (\text{Ger \& Holley, 1976}) \quad (30)$$

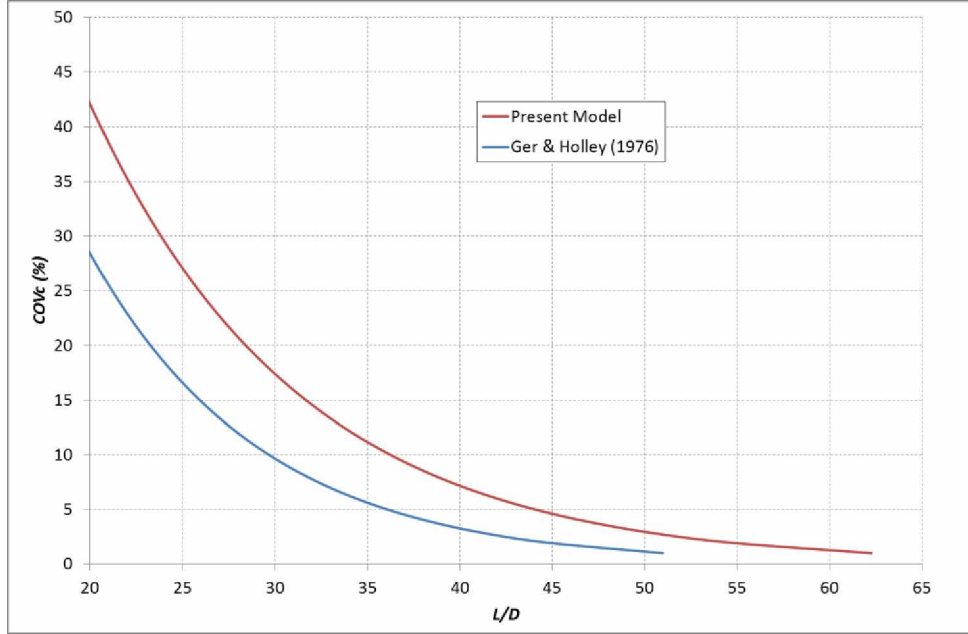


Figure 23: comparison between the present model of Well Mixing Length and those of Ger & Holley (1976) (Re = 50,000)

In Figure 23, the present model calculates a COV greater than that of the Ger & Holley's model. This difference can be explained by the use of different diffusion coefficient values between both studies. Indeed, in their study, Ger & Holley defined the following diffusion coefficient:

$$D_t = \frac{0.071RU_f}{Sc_t} \quad (31)$$

which is greater than the value considered in our model (Equation (22)).

From a safety point of view, the present model is stricter than the Ger & Holley's model. Indeed, if a COV_c of 5% is considered, the Ger & Holley's model recommends a length z^* of around 36, compared to around 45 for the present model.

This approach is useful, especially when dimensioning an installation. However, in most cases the installations have already been built and the duct lengths are often too short to satisfy the "Well Mixing Length". In this situation, it can be interesting to assess the error made if this length is not met. The variation coefficient is therefore no longer relevant. As the sample is a local measurement, another criterion must be considered, namely the difference between the local measured concentration and the expected homogeneous concentration. This criterion noted σ_c is defined by:

$$\sigma_c(z^*, r^+) = \frac{c(z^*, r^+)}{c_H} - 1 \quad (32)$$

By integrating the equation (26) into the equation (32), the criterion is expressed by:

$$\sigma_c(z^*, r^+) = \exp\left(-2 \times \frac{0.058}{Sc_t} a_1 \sqrt{\frac{\lambda}{8}} z^*\right) \frac{J_0(r^+ \sqrt{a_1})}{[J_0(\sqrt{a_1})]^2} \quad (33)$$

and by inverting it, the length z^* for any r^+ can be defined by:

$$z^*(r^+) = \frac{L}{D} = 0.587 \cdot Sc_t \sqrt{\frac{8}{\lambda}} \cdot \ln \left(\frac{617.8}{\sigma_c(\%)} \cdot J_0(r^+ \sqrt{a_1}) \right) \quad (34)$$

and especially for $r^+ = 0$ (duct axis), the equation is reduced to:

$$z^* = \frac{L}{D} = 0.587 \cdot Sc_t \sqrt{\frac{8}{\lambda}} \cdot \ln \left(\frac{617.8}{\sigma_c(\%)} \right) \quad (35)$$

From the equation (34), if a sampling is defined anywhere in a duct, the criterion σ_c at this sampling point can be known and included in the filter efficiency calculation. This is shown in Figure 24, which presents the evolution of the criterion σ_c according to the dimensionless distance $\frac{z}{D}$ for different r^+ ranging from 0 (duct axis) to 1 (duct wall) with a step of 0.1.

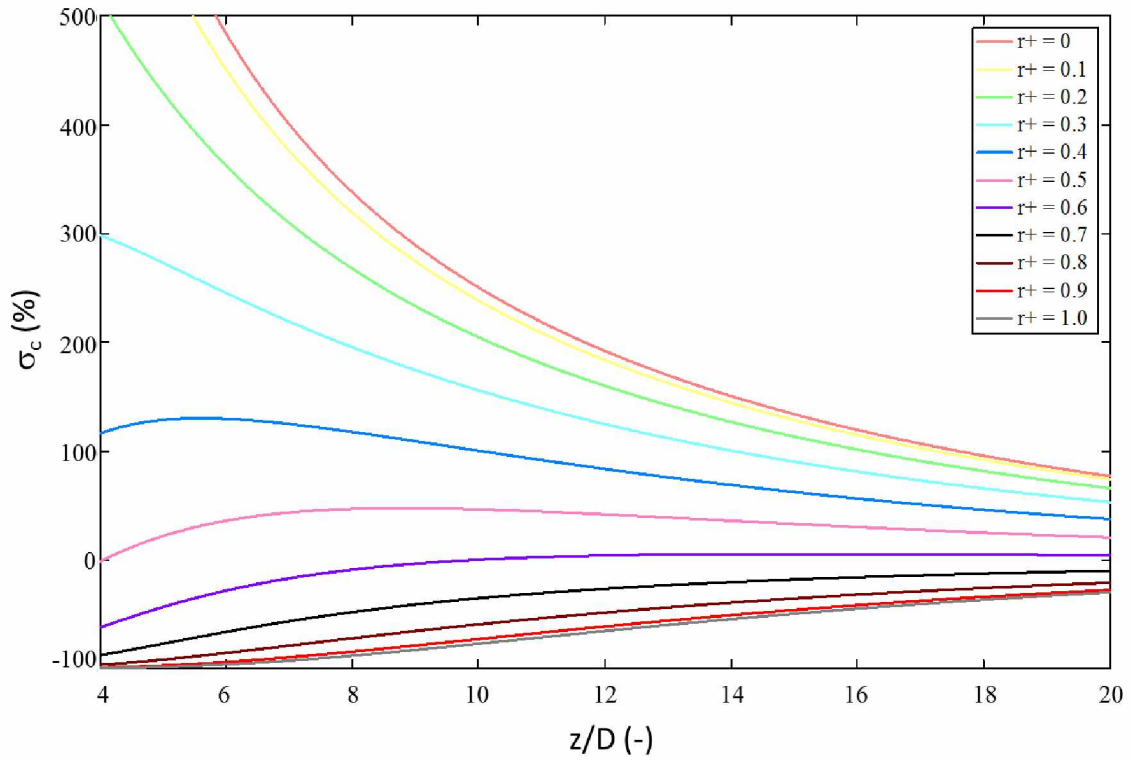


Figure 24: longitudinal evolution of the difference between local measurement and homogeneous concentration for different radial positions

In this figure, it is important to note that the most restrictive sampling is the one at the duct center. Indeed, if a difference of 100 % is considered on Figure 24 and the sampling must be performed at the center of the duct ($r^+ = 0$), a distance of around 20 D is needed, while with a sampling at $r^+ = 0.4$, a length of 12 D is sufficient.

By observing the evolution of these curves, it appears that an optimum location exists to minimize the difference between the homogeneous concentration and the measured concentration and this location is around $r^+ = 0.6$.

6 CONCLUSION

This article presents the development and the validation of a model describing the spatial evolution of a tracer concentration in a cylindrical duct for an injection as a source point at the duct center. To reach this objective, an experimental device has been set up and a specific optical measurement technique has been developed in order to measure the evolution of a tracer in the device at each point of the duct.

The model development based on the resolution of the spatial convection-diffusion equation of a tracer allowed obtaining a first correlation by taking into account several assumptions (Schmidt number, averaged eddy viscosity profile). This model has been compared to experimental data collected on a dedicated experimental bench and validated for a Reynolds number range between 35000 and 100000 and distances from the injection point up to 30 D. However, in order to be easily applied in an industrial context, this model had to be simplified, for achieving two simple correlations: the first one linking the non-dimensional distance Z^* to the global variation coefficient in the section and allowing to evaluate the mixing distance necessary in function of the homogeneity percentage wanted, and the second one linking the same distance Z^* to a local homogeneity criterion σ_c allowing to find the optimum location of a sampling point in order to minimize the difference between the local measured concentration and the homogeneous concentration. The latter correlation also allows to evaluate the error on the measured concentration at a specific sampling point and to take it into account in the uncertainty calculations.

Nomenclature

a, b	Integration constants (-)
C	Concentration (kg.m^{-3})
C_H	Homogeneous concentration (kg.m^{-3})
C_{max}	Injection or maximal concentration (kg.m^{-3})
COV	Coefficient of variation (-)
D	Duct diameter (m)
D_m	Molecular diffusion coefficient ($\text{m}^2.\text{s}^{-1}$)
D_t	Turbulent diffusion coefficient ($\text{m}^2.\text{s}^{-1}$)
GL	Gray level (-)
GL_{max}	Maximal gray level (-)
i	Distance from the inlet point of the laser beam
I_a	Attenuated signal intensity
I_i	Incident signal intensity
J_n	Bessel function (-)
L	Duct length (m)
q_{inj}	Tracer injection mass flowrate (kg.s^{-1})
Q_f	Air flowrate (kg.s^{-1})
M_k	Distribution moment
Pe_t	Turbulent Peclet number (-)
r	Radial location in the duct (m)
r^+	Dimensionless radial location in the duct (m)
R	Duct radius (m)

Re	Reynolds number (-)
U_d	Flow velocity (m.s^{-1})
U_f	Friction velocity (m.s^{-1})
U_{inj}	Injection velocity (m.s^{-1})
U_{max}	Maximal velocity (m.s^{-1})
u	uncertainty (-) or velocity (m.s^{-1})
u_z	longitudinal velocity (m.s^{-1})
z	Longitudinal location in the duct (m)
z^+	Dimensionless longitudinal location in the duct

Greek letters

β	Attenuation coefficient (m^{-1})
θ	Angular coordinate (rad)
κ	Von Karman constant (-)
λ	Friction factor (-)
ρ	Density (kg.m^{-3})
σ_c	Heterogeneity criterion (-)
Sc_t	Turbulent Schmidt number (-)
ν_t	Eddy viscosity (Pa.s)

References

- Anand, M., McFarland, A.R., Rajagopal, K.R. (2003). Gas mixing for achieving suitable conditions for single point aerosol sampling in a straight tube: experimental and numerical results. *Health Physics* **84**(1), 82-91.
- Clayton, C.G., Ball, A.M., Spackman, R. (1968). Dispersion and mixing during turbulent flow water in a circular pipe. *AERE-R 5569*, Isotope Division, Wantage Research Laboratory, Wantage, Berkshire, UK.
- Colebrook, F. (1939) Turbulent flow in pipes with particular reference to the transition region between the smooth and rough pipe laws. *Journal of the Institution of Civil Engineering*, **4**, 14-25.
- Evans, G.V. (1967). A study of diffusion in turbulent pipe flow, *Journal of Basic Engineering*, American Society of mechanical Engineers, Paper 66-FE-A.
- Fitzgerald, S.D., Holley, E.R. (1979). Jet injections for optimum mixing in pipe flow. *WRC Research Report No 144*.
- Frاندolig, J.E., Fahien, R.W. (1957). Mass transfer in low velocity gas streams. *Report of Ames Laboratory*, Iowa State College.
- Ger, A.M., Holley, E.R. (1974). Turbulent jets in crossing pipe flow. *Civil Engineering Studies*, hydraulic engineering series no. 30, 731-745.
- Ger, A.M., Holley, E.R. (1976). Comparison of single-point injections in pipe flow. *Journal of the Hydraulics Division*, 731-745.
- Guo, J., Julien, P.Y. (2003). Modified log-wake law for turbulent flow in smooth pipes, *Journal of Hydraulic Research*, **41**(5), 493-501.
- Gupta, R. (1999). Turbulent mixing and deposition studies for single point aerosol sampling, *Dissertation*, Texas A&M University.

- Jordan, D.W. (1960). A theoretical study of the diffusion of tracer gas in an airway. *Quarterly Journal of Mechanics and Applied Mathematics* **14**(2), 203-222.
- Laufer, J. (1954). The structure of turbulence in fully developed pipe flow, *NACA Report* **1174**.
- Lynn, S., Corcoran, W.H. and Sage, B.H. (1957). Material transport in turbulent gas streams: radial diffusion in a circular conduit. *A.I.Ch.E. Journal* **3**(1), 11-15.
- Mizushima, T., Ogino, F. (1970). Eddy viscosity and universal velocity profile in turbulent flow in a straight pipe, *Journal of Chemical Engineering of Japan*, **3**(2), 166-170.
- Nunner, W. (1956). Wärmeübergang und Druckverlust in rauhen Röhren, *VDI-Forschungsheft*, p455.
- Quarmby, A., Anand, R.K. (1969). Non-axisymmetric turbulent mass transfer in a circular tube. *Journal of Fluid Mechanics* **38**(3), 457-472.
- Reichardt, H. (1951). Vollständige Darstellung der turbulenten Geschwindigkeitsverteilung in glatten Leitungen, *Zeitschrift für Angewandte Mathematik und Mechanik (ZAMM)*, **31**(7), 20-219.
- Roley, G., Fahien, R.W. (1960). Gaseous diffusion at moderate flow rates in circular conduits. *Report of Ames Laboratory, Iowa State College*.
- Seo, Y., McFarland, A.R., Ortiz, A.C., O'Neal, D.L. (2006). Mixing in a square and a rectangular duct regarding selection of locations for extractive sampling of gaseous contaminant. *Health Physics* **91**(1), 47-57.
- Taylor, G.I. 1954. (1954). The dispersion of Matter in turbulent flow through a pipe. *Proceedings of the Royal Society, London, England, Series A, Vol. 223*, p 446.